Contents lists available at Egyptian knowledge Bank (EKB)

Al-Azhar Journal of Agricultural Engineering

journal homepage: https://azeng.journals.ekb.eg/

ORIGINAL PAPER

Development and simulation of a solar power system utilizing PV SYST software

Youssef F. Elsaadawi [a,] ✉, Mohamed M. M. Geasa [a], Enas L. A. Salem [b], Elwan A. Darwish [a]

[a] Department of Agricultural Products Process Engineering, Faculty of Agricultural Engineering, Al-Azhar University, Cairo, Egypt.

[b] Agricultural Engineering Research Institute, Agricultural Research Center, Egypt.

ARTICLE INFO

Handling Editor - Dr. Mostafa H. Fayed

Keywords:

PV panels
PV systems
Solar energy
Simulation
PV SYST

Agricultural Products Process Engineering

ABSTRACT

The abundance of solar energy always coexists with the scarcity of other energy sources and clean water, such as in desert areas. Research articles published in peer-reviewed journals that address the design and simulation of water-pumping systems using PV SYST software are in short supply. Therefore, this study was conducted to design and simulate a 101.4 kW PV underground water pumping system using PV SYST software, with the aim of supplying a farm facing water and energy resource shortages with the necessary water for agricultural facilities and the farming process. Additionally, by simulating the system for a full year using the PV SYST, gathered information about the system's losses, inappropriate components, and design errors. By addressing these issues before installation, time, effort, and resources can be saved. The effective solar radiation value on the collector plane was 2145 kWh/m^2, whereas the nominal power was 461.46 kWh/m^2. This shows the efficiency of the array, which was 21.5% under standard test conditions (STC). The nominal energy of the array was 217810 kWh, whereas the hydraulic energy was 120274 kWh. This difference is due to losses, the most important of which are array losses owing to high temperatures at a rate of 9.83% and converter losses during operation at a rate of 3.21%. The pump's operating electrical energy was 165414 kWh, and its hydraulic energy was 120274 kWh, resulting in a pump efficiency of 72.7 %. The pumped water volume reached 370570 m^3/year, while the water requirement was 370475 m^3/year, indicating that the system was able to meet the water requirements. The performance ratio was 74.1%, which is deemed satisfactory. This signifies the validity of the design and dependability of the PV-powered water pumping system.

1. Introduction

Water is required for large-scale use such as drinking, daily household tasks, irrigation, buildings, and hydroelectric power generation. The growth capacity of a country depends heavily on the amount and quality of water accessible within its limits. There is plenty of fresh water, but it is not easily available. According to the World Health Organization's Global Water Supply and Sanitation Assessment Global Report, 1.1 billion people around the world are unable to access safe drinking water, and this number is expected to increase to 3 billion by 2025. To transport water from the deep Earth's surface to its required location, a pump is necessary. Therefore, water pumps have been used for decades (Verma et al., 2021). The world's energy consumption is rising significantly, due in large part to improvements in living standards and industrial growth in many nations. The gap between the amount of energy generated and consumed has increased. Furthermore, the fuel reserves are gradually being depleted. Additionally, the use of conventional energy-producing technologies contributes to global environmental contamination. These motivations drive scientists to find

✉ Corresponding authors.
E-mail addresses: dr.youssef@azhar.edu.eg (Youssef F. Elsaadawi)

https://doi.org/10.21608/AZENG.2025.373634.1033
Peer review under responsibility of Faculty of Agricultural Engineering, Al-Azhar University, Cairo, Egypt.
Received 15 May 2025; Received in revised form 26 May 2025; Accepted 31 May 2025
Available online 30 June 2025

sustainable, renewable, and alternative energy sources (Ardizzon et al. 2014, Elbelkemy et al., 2025). Energy sources significantly impact a country's economic progress. Globalization and industrialization have depleted nonrenewable energy sources. All nations are currently searching for alternative energy sources, with solar energy becoming increasingly popular worldwide. Solar energy can be intercepted at $1.8*10^{11}$ MW, far more than humans need. Furthermore, it is a clean and reliable source of energy with the ability to meet future demand. It is possible to use solar energy directly to produce thermal and photovoltaic energy or indirectly to generate biomass, wind, waves, hydropower, marine currents, and ocean thermal energy (Ahmed et al., 2020). These days, producing electricity through photovoltaic systems is becoming increasingly common. The scarcity of other energy sources, such as fossil fuels, is the primary cause of this increase. Therefore, switching to dependable and sustainable resources is necessary, like photovoltaic systems. It turns sunlight's limitless energy into electrical energy (Ahmed et al., 2023). Solar energy is a renewable, environmentally favorable energy source. Furthermore, photovoltaic systems (PV) are the most widely used method for directly converting solar energy into direct current. PV water pumping systems (PVWPS) are one of the most common applications for PV power systems, harnessing electricity from photovoltaic panels to power a pumping system, catering to various water pumping needs, such as drinking water and irrigation. A well-constructed PVPS can be efficient and cost-effective in comparison to grid-connected or diesel generator (DG)-based pumping frameworks, especially in rural areas (Muhsen et al., 2017). The bulk of affordable water pumps use either electricity or fuel. This presented a challenge for water distribution to rural areas not directly linked to a national grid station. In addition, as researchers grew more aware of the detrimental environmental effects of burning fossil fuels, they became increasingly focused on constructing freestanding water pumping devices driven by renewable energy sources. Water pumps may get their electricity from a number of renewable energy sources. However, solar photovoltaic (PV) technology turned out to be the most suited. Studies have demonstrated a direct correlation between solar energy and water consumption, despite its clean and readily available nature. Solar intensity is ideal in many areas in which the electrical network does not reach, and there is a significant demand for water (Aliyu et al., 2018). When facing southward, or the equator, in the Northern Hemisphere, the solar conversion mechanism operates at its finest. In the Southern Hemisphere, face northward (Azimuth = 180°). The ideal slope angle depends on the day of the week and your latitude. In Egypt, $\beta opt = \varphi°$ is the ideal fixed tilt angle for photovoltaic modules and collectors to harvest solar energy (Tayel et al., 2022). A variety of factors can influence the total efficiency of a photovoltaic system, including the material of the solar cells, installation technique, the system orientation or tilt, photovoltaic cell layout, and the surrounding climate. As a result, it is critical to study or assess the elements that impact a PV system's capacity to generate power. While manual analysis remains possible, technological advancements have facilitated the creation of various simulation tools like Homer Pro, PV Planner, PVsyst, and others. These programs have demonstrated to be speedy and sophisticated (Samuel et al., 2021). PVsyst is one of the most extensively used simulation applications. Andre Mermoud & Co., Swiss scientists, invented and designed the software. Many engineers worldwide use this software due to its convenience and speedy results. It conducts extensive and detailed research on a wide range of aspects that affect a system's efficiency (Dirnberger 2017). Furthermore, it has the ability to generate reports and provide frequent estimates. The PVsyst software's accuracy is quite near to the actual or true numbers. Other prominent features include color-coded faults and warning messages (Gao, et al., 2016). The PVsyst program simulates a 100 kWp grid-connected solar system, which generates 165.38 MWh yearly but only feeds 161.6 MWh into the grid. The inverter generates 4.42 kWh/kWp of usable energy per day, with an annual performance ratio of around 80% (Kumar et al., 2017). PVsyst conducts the design and performance evaluation of a 2-kW solar photovoltaic system connected to the grid. The daily energy usage is 8.9 kWh, and the hourly load is 2340 W/h, which helps in selecting suitable solar PV modules, batteries, and inverter. The potential solar energy available is 3101.1 kWh, while the customer receives 2962.4 kWh, and their energy needs amount to 3244.8 kWh. The electrical system will gain an extra 33.23 kWh of energy. Most months demonstrate a performance ratio that hovers around 0.7 (Rout and Kulkarni, 2020). The PVsyst simulation tool was used to assess and analyze energy losses along with performance ratios. The plant's average annual energy demand is 1086.24 kWh. While the solar panels generate 1143.6 kWh, the client can only make use of 1068.12 kWh, which does not meet the required load. Various losses resulted in a reduction of the system's power output. The assessment of the performance ratio shows an average PR of 72.8% for the year (Kumar et al., 2021). The PVSyst software was utilized to plan a solar energy system for the selected sites. PV Syst is a well-known software program for modeling and creating PV systems. The photovoltaic pumping system is meant to address issues faced by farmers, such as the need for water for irrigation in India's climate zones, which include combined, humid and warm, dry and hot, moderate, and cold. The values of water pumped are as follows: 1466.8 m^3, 1824 m^3, 2206.9

m^3, 1651.2 m^3, and 1281.3 m^3. This indicates that Jaisalmer had the highest value, whereas Itanagar had the lowest. In temperate climates, the lowest pump efficiency was 57.10%, whereas in hot, dry, warm, and humid climates the highest pump efficiency was 58.60%. The PV array loss was lower in colder areas than in hotter and drier ones. The system experiences losses between 0.27 and 0.37 kWh/kWp/day. Hot and arid conditions lead to greater losses for the system compared to composite factors. Jaisalmer, characterized by its hot and dry climate, exhibits the highest performance ratio, whereas Bangalore, situated in a moderate zone, displays the lowest performance ratio. The performance ratio falls within the range of 0.514 to 0.739 (Yadav et al., 2024).

The objective of this research was to create a 101.4 kW solar photovoltaic water pumping system to extract water from a deep borehole for a farm located in the desert, far from clean water supplies and the national electrical grid. Conducting a system simulation with PV SYST to identify defects, issues, and losses before installation. Assess the dependability and effectiveness of the PV pumping system year-round. There are limited studies available in peer-reviewed journals regarding the design and simulation of photovoltaic (PV) water-pumping systems using PVSYST software. This study's primary contribution is to outline a simple and reliable method for constructing and simulating PV water-pumping systems. Moreover, this analysis confirms the efficiency, dependability, and possible problems of the system before installation, thereby reducing the effort and cost and preventing the development of technical problems that can compromise or cause failure of the system after installation.

2. Materials and methods

A solar energy system with a capacity of 101.4 kW has been designed and simulated to provide power to a 75-kW submersible pump located in Egypt, specifically at a latitude of 28.5 N, longitude of 30.0 E, and an elevation of around 119 m above sea level. The geographic location of the project is shown in Fig. 1.

Fig. 1. The geographical location of the project.

2.1. Materials

Five major components make up the photovoltaic water pumping system: PV modules, an inverter, a submersible pump, a steel structure, and additional electrical equipment (such as protective devices, cables, and MC4).

2.1.1. Photovoltaic panels

To energize the water pumping system, 169 photovoltaic modules were installed. The used JA (JAM78S30-600MR) depicted in Fig. 2. possesses a rated power of 600 watts. Table 1presents the datasheet for the PV module.

Fig. 2. JA (JAM78S30-600MR) photovoltaic module.

2.1.2. Variable frequency drive (inverter)

The photovoltaic (PV) modules produce direct current (DC) electricity, which the inverter then transforms into alternating current (AC) power to operate the pump motor. Additionally, it automatically adjusts the output frequency to align with the existing radiation levels. Furthermore, it employs Maximum Power Point Tracking (MPPT) technology to enhance power output across the entire spectrum (Tayel et al., 2019; Elwakeel et al., 2021). Fig. 3 displays the 75-kW inverter (Veichi IS23, MPPT). Table 2 provides the specifications of the inverter.

2.1.3. The pumping unit

The pumping unit consists of three essential elements: a deep borehole, a multistage submersible pump, and a three-phase alternating current motor. Table 3 provides the specifications for the Vansan VSM 8/100 submersible three-phase electric motor. Table 4 outlines the technical specifications for the Vansan VSP-SS 08125/07 centrifugal submersible pump, and Fig. 4 illustrates the performance curves.

Table 1

JA(JAM78S30-600MR) PV module data sheet.

Model type	JA (JAM78S30-600MR)
Max Power (P Max)	600 W
Voltage at Max Power Point (Vmp)	45.3 V
Current at Max. Power Point (imp)	13.25 A
Open Circuit Voltage (Voc)	53.5 V
Short Circuit Current (Isc)	14.03 A
Normal Operating Temp. (NOCT)	45℃ (±2℃)
Panel Dimension (mm)	2465 ×1134× 35
Panel Weight (Kg)	31.1 kg (Approx.)
Max. Series Fuse	25 A
Max. System Voltage	1500 VDC
Module Efficiency STC	21.5 %

Fig. 3. Veichi IS23, 75-kW inverter.

Table 2

Veichi IS23, 75-kW inverter datasheet.

Model	Veichi IS23 T3
Nominal Power	75 kW
Voltage output	380 (V)
Peak output current	150 (A)
Peak input power	115 (KW)
Peak input voltage	800 (VDC)
MPPT voltage range	350-750 (VDC)
Frequency	0-600 (Hz)

Table 3

The technical specifications of the 3-phase VSM 8/100 motor

VSM 8/100	Type
75	Power- kw
380	Volt- v
150.7	Current- A
50	Frequency-HZ
84 %	Efficiency
Φ=192, L =1366	Dimensions-mm
0.88	Cos φ

Table 4

The technical specifications for the Vansan VSP-SS 08125/07 pump.

Type	Stages	Flowrate	weight	Revolution	Dimensions (mm)		
					L	Φ	Shaft Φ
VSP-SS 08125/07	7	100-145 m^3/h	71 kg	2900 rpm	1620	213	30

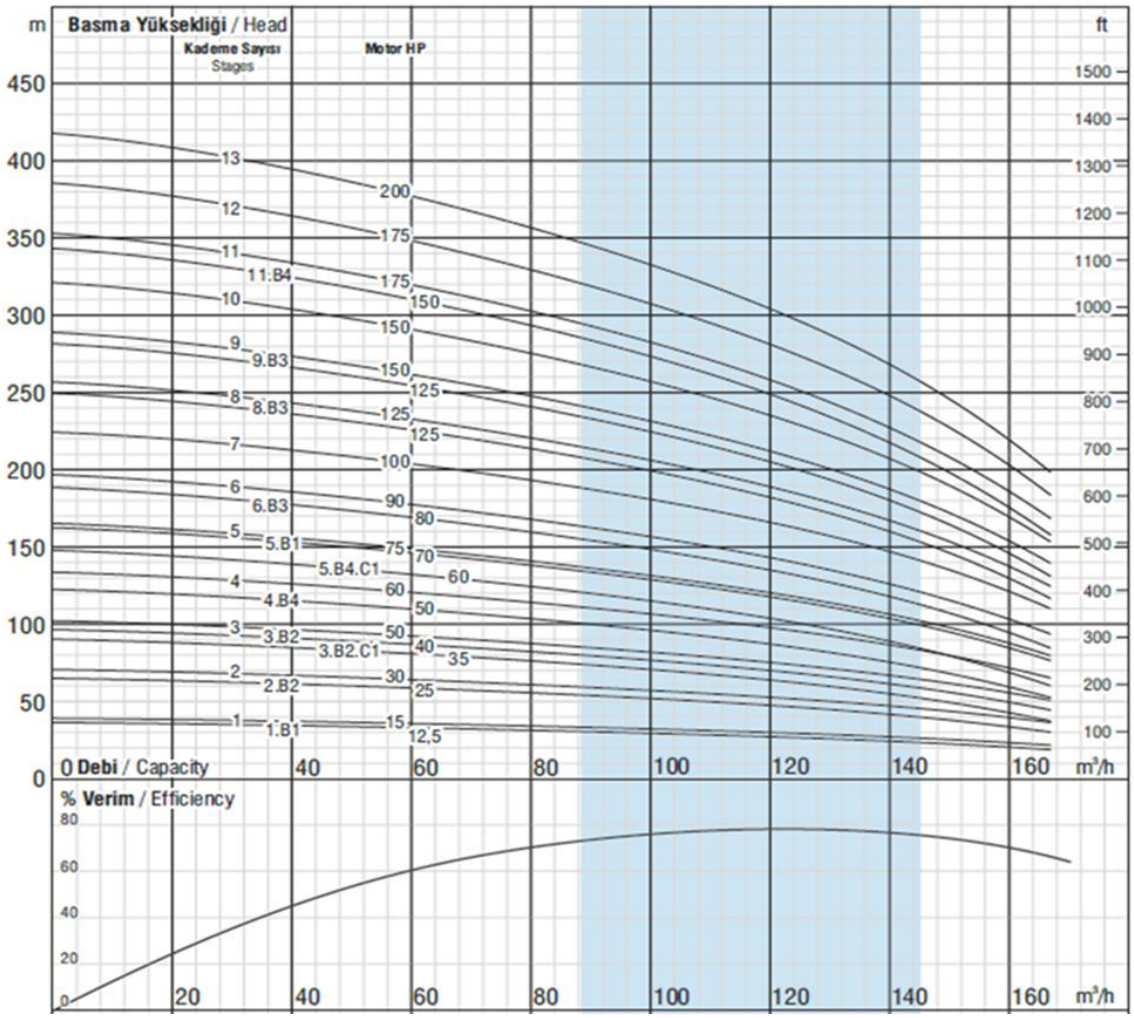

Fig. 4. The Vansan VSP-SS 08125/07 pump performance curves.

2.1.4. Aquifer and borehole specifications

According to the Ministry of Water Resources and Irrigation, the groundwater in the project area is located in the Eocene cracked limestone aquifer, which is considered one of the largest limestone aquifers in Egypt, with an average thickness of approximately 400 m and a static water surface depth of 70–110 m. This aquifer is characterized by an acceptable salinity of 2–3 g/L. These specifications are considered beneficial for establishing sustainable agricultural development projects. Table 5 displays the borehole's technical specifications.

Table 5

Well Specifications.

Land level above sea level	109.52 m
Total depth of the well	610 m
Static level	72 m
Pumping rate during pumping experiment	180m^3/h
Pumping experiment time	24 hr.
Reservoir loss factor B	0.0609 h/m^2
Maximum well drawdown	35.38 m
Safe flowrate	150 m^3/h
drawdown corresponding to safe pumping	26.4 m
Salt concentration	2176 mg/Lit.
Coordinates	30 ℉, 28 ℕ

2.1.5. PV System Setup

Fig. 5 gives an illustration of the primary components of the system, as well as the linking strategy and the working theory, as they are read and defined by simulation software. The system consists of a solar array of 169 panels (13 panels in series, 13 strings in parallel). The array supplies the inverter with the appropriate voltage (588.9 volts) and current (172.25 amps) to operate efficiently (MPPT). The inverter (Veichi IS23, 75 kW) controls a 3-phase 100 hp motor (VSM 8/100), which drives a 7-stage submersible pump (VSP 08125/07). A 6000 m^3 tank stores water for use at night or during system maintenance stops.

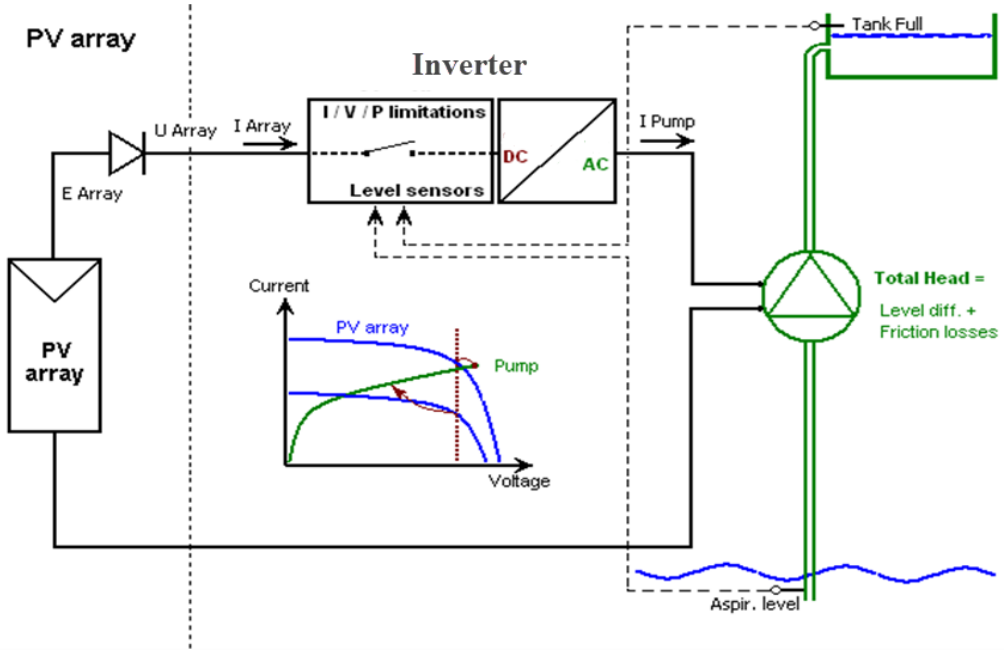

Fig. 5. PV system configuration

2.2. Methodology

Prior knowledge of the characteristics and limitations of each system component facilitates the process of designing and simulating the system; additionally, pre-sizing helps to assemble and prepare most of the data required to create a proper simulation. Overall, it is preferable to create an initial design with calculations before initiating the design and simulation process using PV SYST software. The main advantages of this approach are the assurance of the calculations' accuracy and the design's efficiency. Therefore, we will develop a preliminary design and select suitable components of the system. Next, we will assess the design's validity and efficiency using PV SYST software and then conduct a year-long simulation to assess the system's reliability and analyze the various technical and environmental factors influencing it.

2.2.1. Essential data for system sizing

The dimensions of the pumping pipes, the daily water usage, and the static water level are essential factors to understand throughout the different stages of designing the solar water pumping system. The current specifications are as follows: an average water usage of 1015 m^3 per day, a static water level of 72 meters, a drawdown rate of 0.18 m/m^3/h, pumping pipes that are 150 meters long, and a diameter of 6 inches (152.4 mm).

2.2.2. Pump sizing and selection

To choose the most suitable pump, it's essential to accurately determine the total dynamic head (TDH) in meters and the flow rate (Q) in cubic meters per hour. The friction head (Hf) in meters indicates the pressure loss in the piping system caused by friction. The friction head was calculated using Equation 1 based on the Hazen-Williams formula.

$$H_f = K \times l \times \left(\frac{Q}{C}\right)^{1.852} \times d^{-4.87} \quad \ldots [1]$$

where d is the inner diameter of the pumping pipelines (mm), Q is the discharge (lit/s), l is the length of the pumping pipelines (m), K is the constant coefficient ($1.22*10^{10}$), and Hf is the friction loss (m).

$$h_f = 1.22 \times 10^{10} \times 150 \times \left(\frac{40.28}{150}\right)^{1.852} \times 150^{-4.87} = 4m$$

The total dynamic head (TDH) is the total equivalent height to which water must be raised vertically, considering friction losses in the pipe. Eq. 2 expresses the total dynamic head TDH.

$$TDH = Hst + Hd + Hf + Hp \quad \ldots [2]$$

In this context, Hf denotes friction head (m), Hd represents drawdown head (m), Hp signifies pressure head (m), and Hst indicates static head (m).

$$TDH = 72 + 26.4 + 4 + 30.6 = 133\ m$$

It is necessary to select the right pump from the pump efficiency charts utilizing TDH (133 m) and discharge (145 m^3/h). The efficiency chart specified a 100-horsepower, 7-stage pump.

2.2.3. The variable frequency drive's (VFD) sizing

- The inverter is regarded as the central component of a solar power facility. Selecting the wrong inverter can result in issues or damage to the PV system or the devices that depend on it for energy. Therefore, the following factors must be considered when sizing a pumping inverter (Khamisani 2019; Muzaffar and Iqbal 2020):
- Motor power ≤ inverter power.
- To ensure optimal operation, the PV panel's maximum power voltage (Vmp) must be within the MPPT voltage range of the inverter.
- The open-circuit voltage (VOC) of a solar array needs to be less than the maximum voltage that the inverter can accommodate (Usman et al., 2020; Chandel et al., 2014).

These parameters led to the selection of an inverter with the following features: Veichi SI23 75 kW, pure sine wave, maximum input voltage of 800 V, MPPT voltage range of 350-750 V, and maximum array power of 115 kW. The arrangement of the array's panels may be selected in order to ensure that its output meets the inverter's parameters by referring to the inverter's specifications.

2.2.4. Sizing the photovoltaic array

The panel's output diminished during the morning, overcast, and sunset phases. The power needed to run the pump, multiplied by 1.3, determines the capacity of the photovoltaic array.

PV array power = 1.3 x pump motor power = 1.3 x 100 hp = 130 hp = 130 hp x 746 W = 96980 Watts

Number of solar modules = PV array power / module power (Faiz et al.,2021)

= 96980/ 600 = 161.6 modules ≅ 162 modules

The way in which panels are connected (either in parallel or in series) is determined by the voltage and current requirements for the inverter to operate efficiently. According to the Veichi 100 hp inverter specifications, 13 panels are connected in series to create 13 strings. Each string has a voltage of 588.9 V (calculated as 13 × 45.3 V). The 13 strings are then linked in parallel to produce a total current of 172.25 A (which is 13 x 13.25 A). To meet the inverter's specifications, the number of modules needs to be calculated by multiplying the number of modules in each string by the total number of strings, resulting in a total of 169 modules (Aghaei et al., 2020a).

2.2.5. Sizing cables and wires

When selecting direct current cables, it is imperative to exercise caution, as the improper selection of cables and wires may lead to many issues, including overheating, malfunction, and, in some cases, fires, which may inflict significant damage to the facility or even result in human casualties. The cross-sectional area of the wire or cable may be determined using the voltage drop equation (Ameur et al., 2021).

- The DC wires' cross-sectional area between the array and the combiner box is calculated as follows (Eq. 3):

$$A = \frac{2 \times L \times I \times \rho}{V_d \times V} \quad \ldots [3]$$

- In this equation, A represents the cross-sectional area of the wire (in mm^2), L denotes the length of the wire (in meters), and ϱ signifies the resistivity of the conductor (0.017 Ω.mm^2/m for copper and 0.028 Ω.mm^2/m for aluminum). Vd indicates the voltage drop (which can range from 1% to 3%), while V refers to the voltage across the wire (in volts).

$$A = \frac{2 \times 50 \times 14.03 \times 0.017}{0.03 \times 588.9} = 1.35\ mm^2$$

- Due to its unavailability in the market, the next largest commercially accessible value, 4 mm^2, is used.
- The DC wires' cross-sectional area between the combiner box and the inverter is calculated as follows:

$$A = \frac{2 \times 15 \times 182.39 \times 0.017}{0.03 \times 588.9} = 5.3\ mm^2$$

Because this value is unavailable in the market, the next larger commercially accessible value of 6 mm^2 is used.

- Sizing the DC circuit breaker (located between the combiner box and the inverter) (García et al., 2021; Aghaei et al., 2020b).

DC CB capacity amp. = 1.56 × I_{SC} = 1.56 × 182.39 = 284.5 A

Due to its unavailability in the market, the next larger commercially accessible value, 300 A, is used.

- Sizing the DC string fuses within the combiner box:

Fuse capacity amp. = 1.56 × I_{SC} = 1.56 * 14.03 = 21.9 A

Because this value is unavailable in the market, the next largest commercially accessible value, 25 A, is used.

2.2.6. Simulation software and the design process

The simulation was conducted with the renowned PV SYST 7.4 software. This program enables the design of a variety of solar energy systems, including on-grid, off-grid, and pumping systems. A notable benefit of

using the PV SYST software is its ability to notify the designer of any errors, including minor ones, in the design or selection of system components. It additionally provides essential information regarding the performance and efficiency of the system over the course of the year. A key function of this program is to perform a year-long performance simulation of the system (Rout and Kulkarni, 2020; Kumar et al., 2021). Fig. 6 illustrates the steps involved in utilizing the PVSYST software for the PVWPS design. The design process begins by selecting the geographical site and then defining the collector array orientation. Select the "Water needs" button on the "Pumping Hydraulic Circuit" page to define the pumping circuit, specifically the " pumping water from a deep well to a storage tank" system. On the "Water needs and head definitions" page, specify the water needs in m3/day and the pumping static depth. In the "System" dialog, on the "Pump definition" page, select the pump model. On the "Sub Array Design" page, choose the photovoltaic (PV) module along with an appropriate configuration for the PV array, and establish the number of modules arranged in series or parallel for the design of the PV array. Additionally, you need to select the control mode and controller device. You should open the controller device and check its parameters. No red errors mean you can run your first system simulation. Fig. 7 illustrates the main software interface throughout the design and simulation of PVWPS.

3. Results and discussions

3.1. Sun trajectory and horizon

The azimuth and solar altitude for an annual cycle are represented in degrees by the solar path. The azimuth, measured in degrees clockwise from true north, denotes the horizontal angle of the sun's position. Conversely, the sun's altitude denotes the angle at which it is raised above the horizon. The sun path diagram depicts overlapping lines that represent the sun's trajectories in relation to specific shading conditions (Ramoliya, 2015). The tangential boundaries of the plane, or the locations where the sun's rays are parallel to it, are denoted by blue lines. This illustration provides a simulated assessment of the distribution of shade based on the season and the time of day (Serat et al., 2023). Because the photovoltaic system is located in the Northern Hemisphere, its PV modules should be oriented southerly. The sun path diagram in Fig. 8 clearly indicates that the PV array is appropriately positioned and that the sun maintains a high height above the horizon for most of the year. During the morning, afternoon, and winter, the solar elevation angle is below 35 degrees, and the azimuth angle exceeds 60 degrees. This may cause shade from objects on the horizon.

3.2. The inclination and orientation of the PV array

To achieve optimal production, the tilt angle of the panels is set to align with the local latitude, while the panels face south in the northern hemisphere. PV SYST generates a table containing 475 annual transposition factor calculations for varying tilt angles and azimuth orientations. Subsequently, the tool provides curves for different transposition factors, showcasing "iso-transposition" orientations alongside the best orientation. Each curve also indicates the extent of loss compared to the ideal orientation (El Abagy et al., 2021). The transposition factor refers to the proportion of radiation received on the plane (GlobInc) compared to the horizontal radiation (GlobHor). It indicates a gain (or reduction) when the collector plane is tilted. Fig. 9 demonstrates that the optimal tilt and orientation angles are 28 degrees and 0 degrees, respectively. Furthermore, it indicates that the loss associated with tilt and orientation relative to the optimum is zero.

3.3. Reference Energy Received in the Collector Plane GlobInc [kWh/m²/day]

In the collector plan, the reference incident energy Yr GlobInc (kWh/m²/day) is equal to the ideal array yield based on Pnom as specified by the manufacturer, assuming no losses occur (Yr Normalized Reference nominal energy at STC kWh/kWp/day). To put it another way, the normalized reference nominal energy Yr [kWh/kWp] indicates the electrical energy produced by the reference incident energy on the collector plane under standard test conditions (kWh/m²). There is frequently ambiguity surrounding the units of the quantity Yr, which can be interpreted as either the incident energy presented in units of [kWh/m²/day], or the ideal array yield based on Pnom, measured in units of [kWh/KWp/day]. This numerical equivalence is based on the STC definition: one kWh/m² of irradiance should result in one kWh/kWp of produced electricity. The confusion arises from the fact that the kWh in these two units refer to different concepts; in the first case, [kWh/m²/day], the kWh signifies incident irradiance energy (light flux), whereas in the second case, [kWh/kWp/day], the kWh indicates generated electrical energy (El Abagy et al., 2021; Elsaadawi et al., 2025). Fig. 10 illustrates the reference incident energy measured on the collection plane. In August, the estimated incident energy for the collection plane reached its peak at 6.67 kWh/m²/day, while in December, it fell to its lowest point of 4.79 kWh/m²/day. Over the course of the year, the average reference incident energy on the collection plane was calculated to be 6.029 kWh/m²/day.

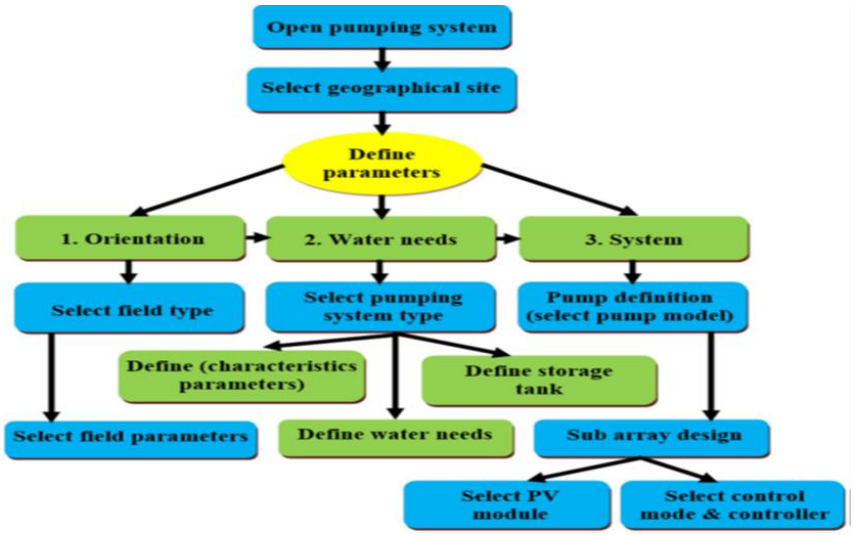

Fig. 6. The process of using PV SYST software [15]

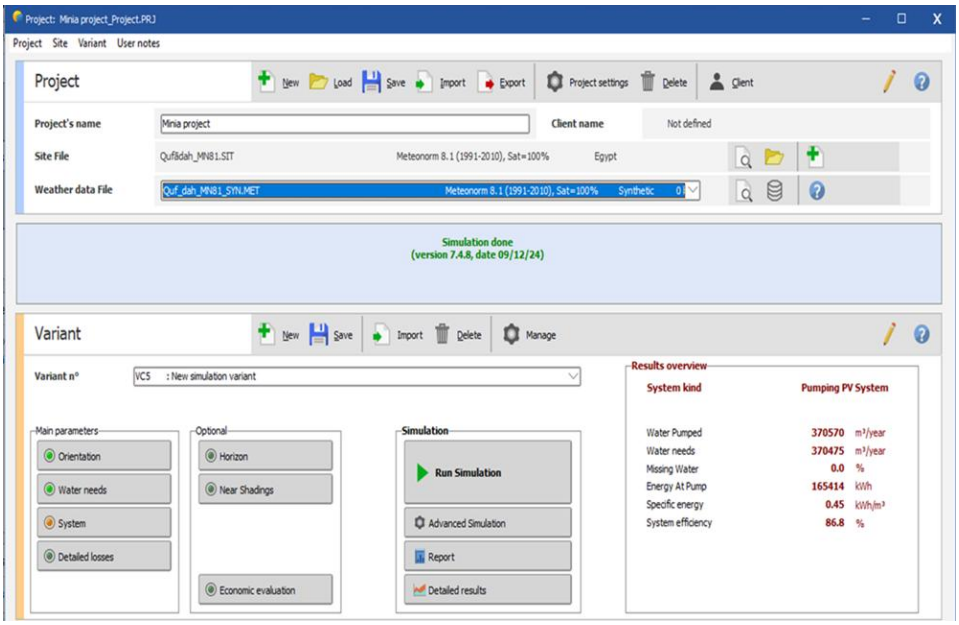

Fig. 7. PV SYST 7.4 during PVWPS design.

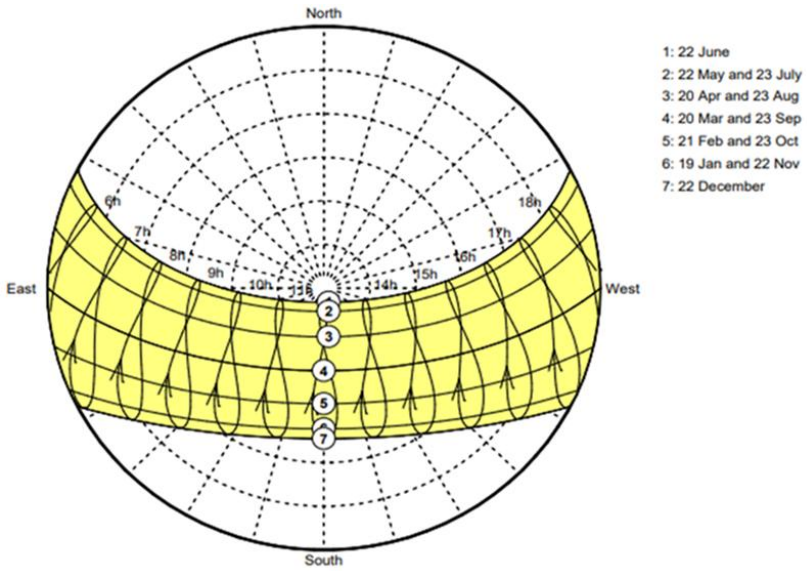

Fig. 8. Sun trajectory and horizon.

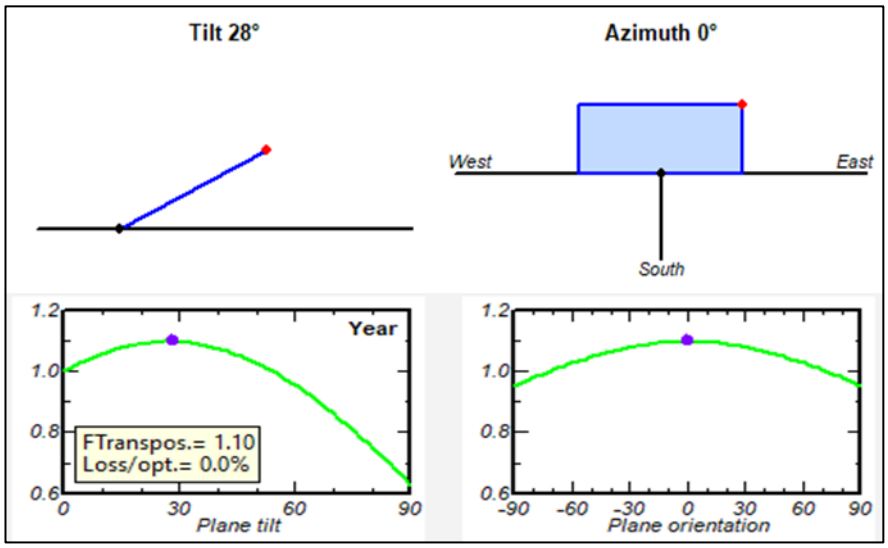

Fig. 9. PV Array tilt and orientation.

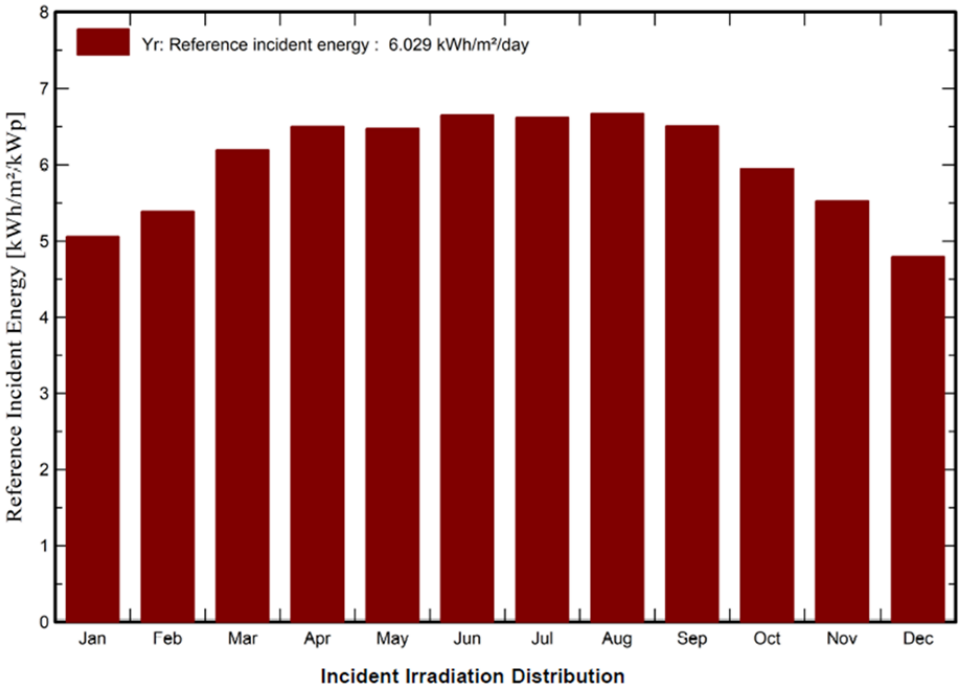

Fig. 10. Reference Incident Energy in the Collector Plane GlobInc.

3.4. Normalized output and reduction factors

The yield of an array, expressed as kWh/kWp/day, is known as daily energy production (Ya). The daily usable energy output of the system, also called system yield (Yf), is measured in kWh/kWp/day. The collection loss (Lc) is defined as the gap between the reference energy incidence on the collector plane (Yr) and the array yield (Ya). This loss encompasses factors such as wiring, thermal properties, module quality, IAM losses, mismatch, dirt, shading, regulation losses, MPP, and additional inefficiencies. System losses (Ls) represent the difference between the array yield (Ya) and the system's daily usable energy, or system yield (Yf). Examples of Ls are inverter losses in photovoltaic water pumping systems and battery inefficiencies in stand-alone systems. Unused energy (Lu) is the hypothetically available energy at the array output that remains unutilized due to system saturation, such as a fully charged battery, restricted load in a DC grid system, or a full tank in a photovoltaic water pumping system (PVWPS). The collection loss (Lc) occurs only when the system consumes the generated energy (Kumar et al., 2017; Espina et al., 2022). The unused energy (Lu) (tank full) reached 0.46 kWh/kWp/day. The collection losses (Lc) or PV array losses of the array were 0.81 kWh/kWp/day. The system losses (Ls) were 0.26 kWh/kWp/day. The unused energy (Lu) with a full tank reached 0.46 kWh/kWp/day. The collection losses (Lc), which are

also referred to as PV array losses, totaled 0.81 kWh/kWp/day. System losses (Ls) were recorded at 0.26 kWh/kWp/day. The final yield (Yf) is defined as the daily useful output energy of the system, indicated in nominal power (kWh/KWp/day) (Nag and Gangopadhyay, 2022). The final yield (Yf) of this system was 4.47 kWh/kWp/day (Fig. 11). Fig. 12 illustrates the normalized production and loss factors represented as percentages.

3.5. Performance Ratio (PR)

The global system efficiency is characterized by the performance ratio (PR), which indicates the ratio of the actual energy produced (Yf) to the energy that would be generated if the system operated continuously at its standard test conditions (STC) efficiency (ideal array yield Yr) (Nag and Gangopadhyay, 2022). In the context of autonomous systems, this pertains to the photovoltaic energy that is delivered efficiently to the pump. The PR accounts for various losses, including optical (such as shading, incident angle modification, and soiling), array losses (like PV conversion, aging, module quality, mismatch, wiring, etc.), and system losses (inverter efficiency in both grid-connected and pumping applications, as well as storage/battery/unused losses in off-grid systems). This indicator functions on its own, unlike the "Specific energy production" indicator that depends on the orientation of the plane and meteorological data, measured in [kWh/kWp/year]. This allows for the evaluation of the quality of systems in installations with various orientations and locations. The PR indicates the availability of solar energy for end-use applications (Kumar et al., 2021; Cosgun and Demir, 2024). Fig. 13 shows the PV pumping system performance ratio (PR) of 0.74.

3.6. Distribution of Incident Irradiation

Fig. 14 shows how global incident irradiance is distributed on the PV system's collector. The histogram represents the distribution of the total global incident energy (kWh per 20 W/m² class) based on the global incident at the collection plane (W/m²). The accumulated global incident energy in the collecting plane (kWh/class of 20 W/m²) is organized into "bins" (bars or classes) based on certain operational circumstances defined along the abscissa (global incident irradiance in the collection plane (W/m²)). A bin or class represents the aggregation of energy for each simulation time step when the global incidence on the collecting plane (W/m²) falls within a specified range, such as between 400 and 420. In this instance, the "bin" ranges from 400 to 420 W/m². The height signifies the cumulative energy received on the collecting plane during the year, during which the global incident energy on the collection plane ranged from 400 to 420 W/m².

3.7. Effective Irradiance and array temperature

The variation in the array's temperature in response to variations in effective irradiance is illustrated in Fig. 15. The average temperature of the array fluctuated between 25°C in winter and almost 60°C in summer, which significantly deviates from the STC values (25°C at 1000 W/m²) (Nag and Gangopadhyay, 2022). Elevated temperatures are unequivocally a significant factor detrimentally impacting solar panel efficiency, with thermal losses constituting 9.83% of the array's nominal output at Standard Test Conditions (STC).

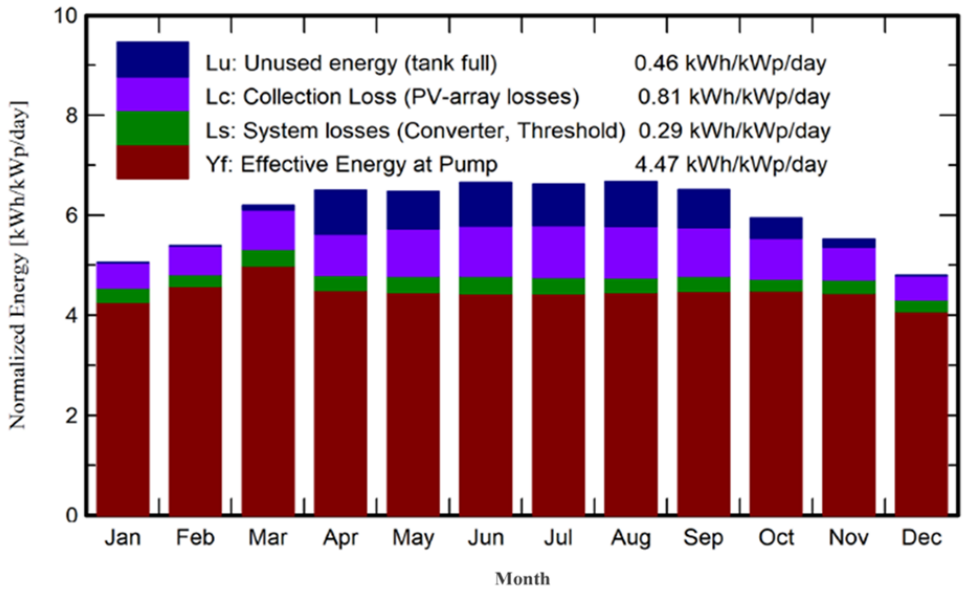

Fig. 11. Normalized productions (kWh/KWp/day).

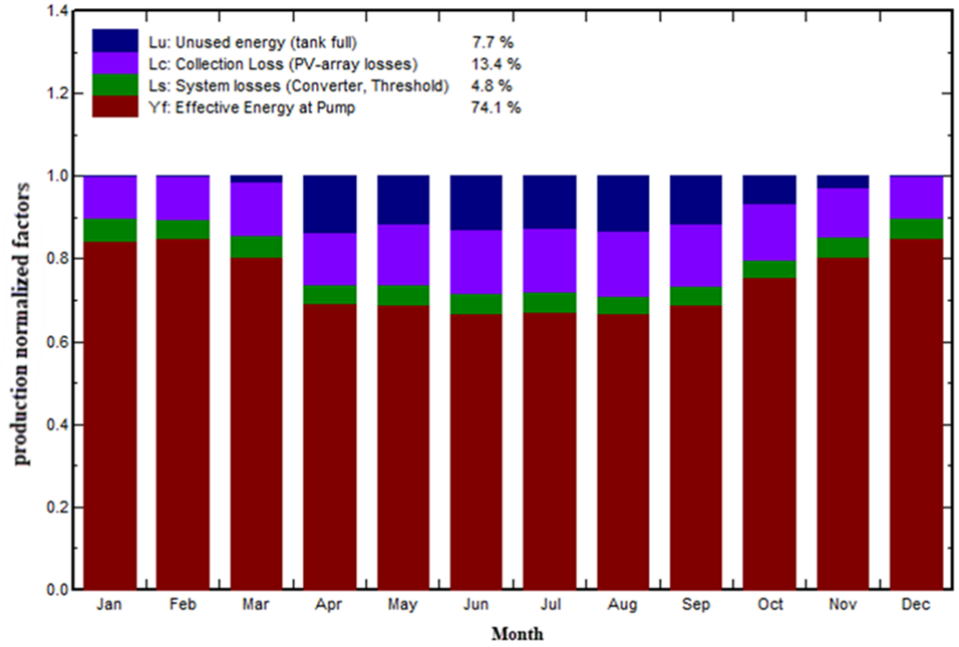

Fig. 12. Normalized production and loss factors, expressed as percentages

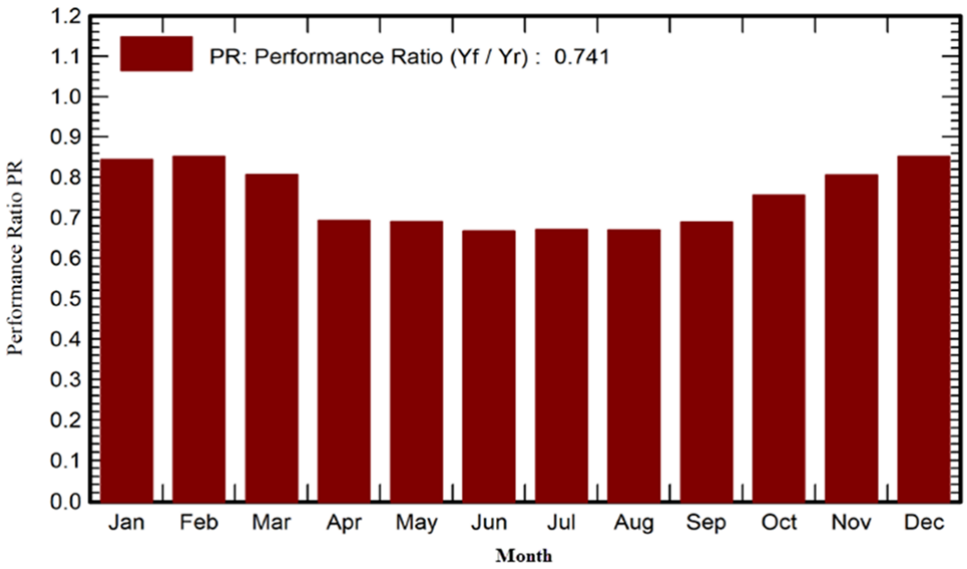

Fig. 13. Performance Ratio PR

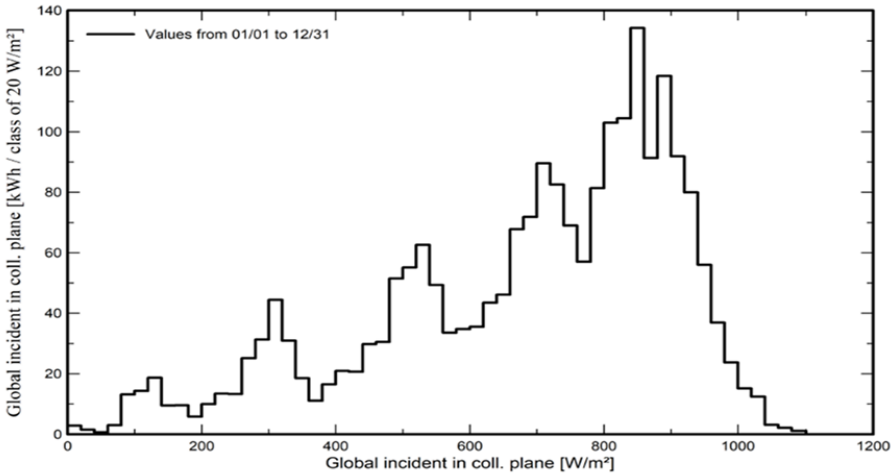

Fig. 14. Incident Irradiation Distribution

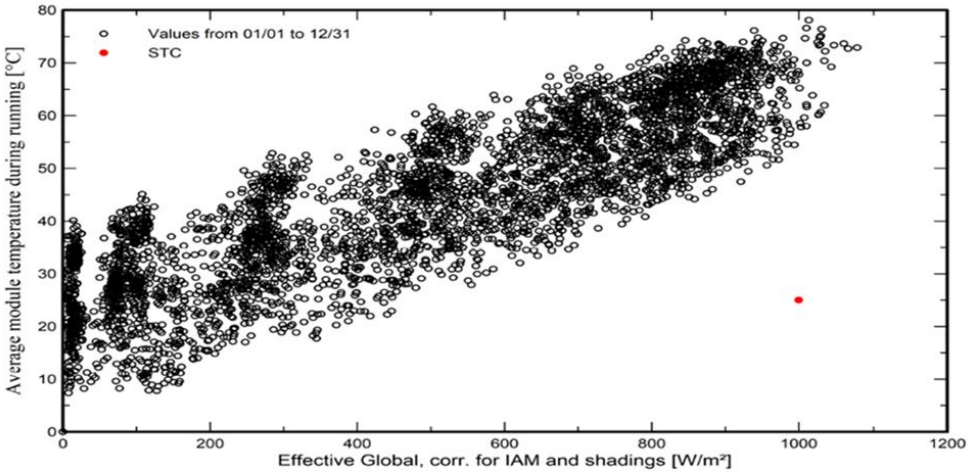

Fig. 15. Array temperature vs. effective irradiance.

3.8. The array's daily input/output

The daily input/output diagram shown in Fig. 16 illustrates the global incident irradiance on the collection surface in kWh/m²/day and the overall effective energy production from the array in kWh/day (Serat et al., 2023). The average global incident irradiance on the collecting surface was measured at 6.03 kWh/m²/day, while the mean effective energy output from the array was 519.20 kWh/day (Abbood Al-Khazzar, 2018). The effective energy production of the array recorded minimum and maximum values of 435.66 kWh/day in December and 559.55 kWh/day in April, respectively, as seen in Fig. 17.

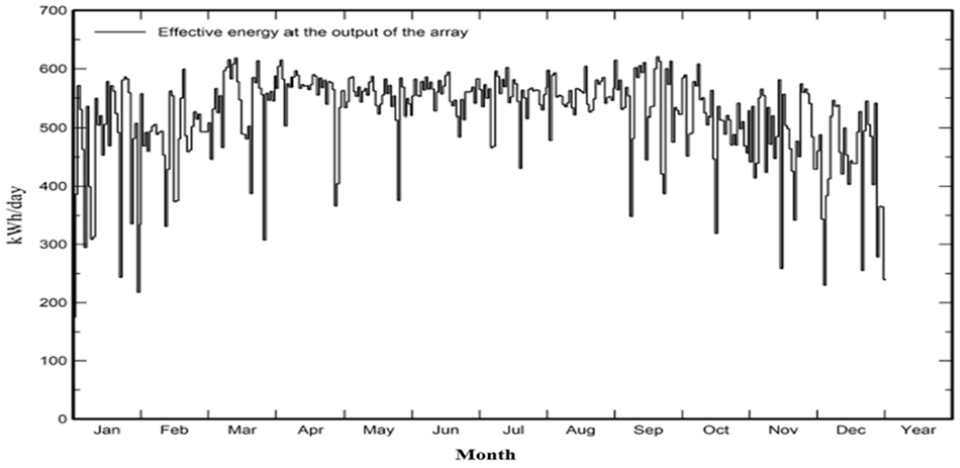

Fig. 16. Daily Input/Output of the array.

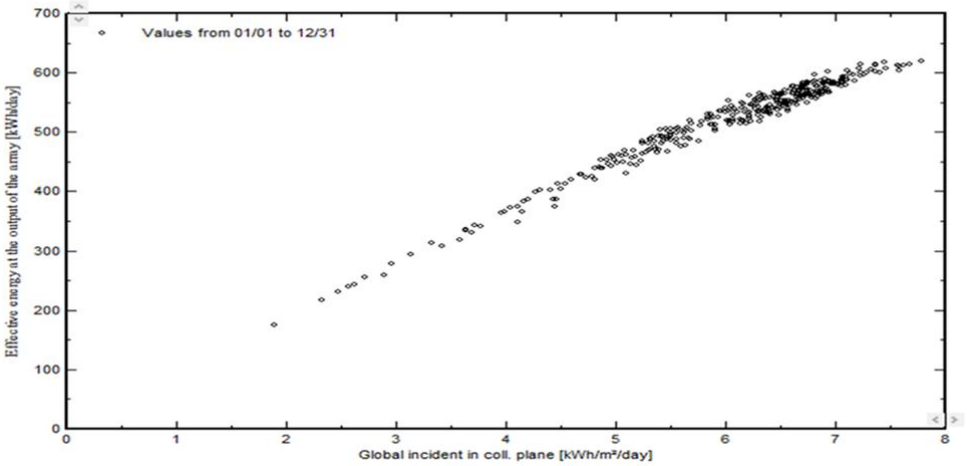

Fig. 17. Daily array output effective Energy.

3.9. Effective array's power distribution

The effective power distribution of the PV array is shown in Fig. 18. The histogram demonstrates how effective energy production from the array is distributed (kWh/class of 1 kW) in relation to the effective power output from the array (W). The total effective energy at the output of the array (kWh/class of 1 kW) is categorized into "bins" (bars or classes) according to a defined operating state illustrated on the horizontal axis (effective output power of the array, kW) (Nag and Gangopadhyay, 2022; Ali et al., 2023). A bin or class represents the aggregation of energy at every simulation step of time when the effective power at the array's output (kW) falls within a specified range, such as between 30 and 31. In this instance, the "bin" ranges from 30 to 31 kW. Its height signifies the total effective energy production of the array (kWh per class of 1 kW) during the year, while the effective power output of the array (kW) ranged from 30 to 31 kW.

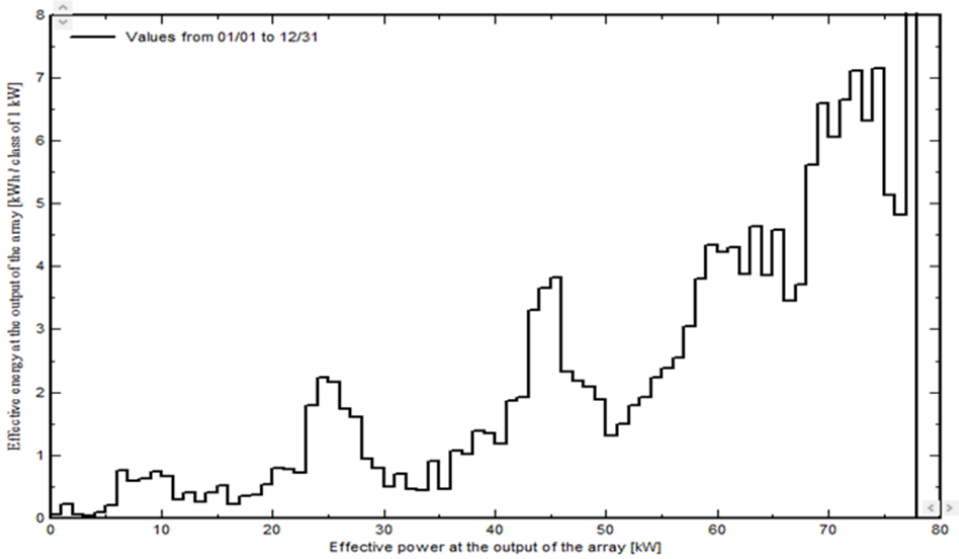

Fig. 18. Array effective power distribution.

3.10. Efficiency, I-V, and P-V of PV panels

The I-V and P-V charts depict the various voltage-current and voltage-power values for a specific module. These curves are key indicators of the module's performance. From the I-V and P-V graphs, crucial values can be determined, such as the open-circuit voltage (VOC), short-circuit current (ISC), and maximum power point (Pmax). Open-circuit voltage (Voc) is defined as the maximum voltage when no current is being drawn from the module. The short-circuit current (ISC) represents the current that flows through the solar module when the voltage is at zero or when the solar cell is shorted. The maximum power point (MPP) is identified as the point at which the product of voltage and current reaches its highest values (Elsaadawi et al., 2023). Fig. 19 shows the I-V curves as a function of different irradiance levels: the VOC and ISC equal 50.28 V and 14.17 A, respectively, at 1000 W/m² and 45 °C. Fig. 20 illustrates the P-V curves, where Pmax and Vmax equal 558.7 W and 41.5 V, respectively, at 1000 W/m² and 45 °C. Fig. 21 illustrates the efficiency curves at various levels of solar radiation and temperature. Elevated temperatures have an adverse effect on solar panels; thus, when solar radiation reaches 1000 watts/m² and the temperature rises to 70 °C, the efficiency drops to 18%. In contrast, at a temperature of 40 °C, the efficiency improves to 20.4%, highlighting the considerable negative influence of high temperatures on solar energy systems. The maximum power and panel efficiency values were 600 W and 21.5%, respectively, at 1000 w/m² solar radiation and 25 °C.

3.11. Variable frequency drive efficiency

The inverter is considered an essential element of the system, acting as a critical connection between other components and frequently described as its core. It converts direct current to alternating current and operates at a variable frequency to optimize the yield of fluctuating solar radiation, particularly during the morning, evening, and winter. The efficiency of the inverter directly influences the energy output of the system in a linear manner. Thus, optimal system performance necessitates great efficiency over the whole power spectrum. The inverter's efficiency, representing the proportion of input power converted to output, is contingent upon the input voltage, input power, and the load fraction imposed on the equipment. Fig. 22 illustrates the inverter efficiency, which attained 96%, signifying that the inverter was subjected to suitable inputs and outputs from the panels and loads (Ramoliya, 2015).

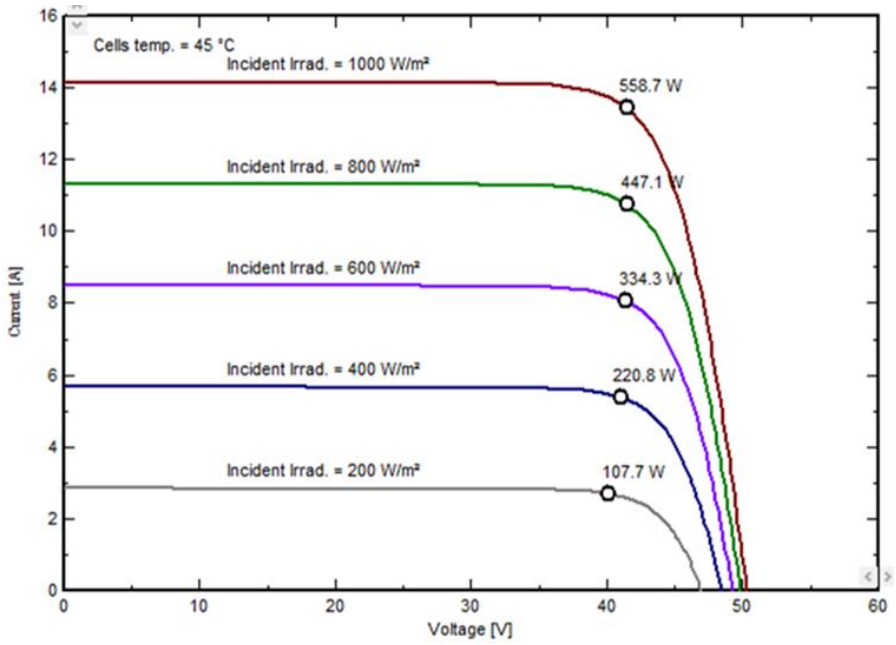

Fig. 19. JA (JAM78S30-600MR) photovoltaic module current-voltage characteristics at various levels of irradiance.

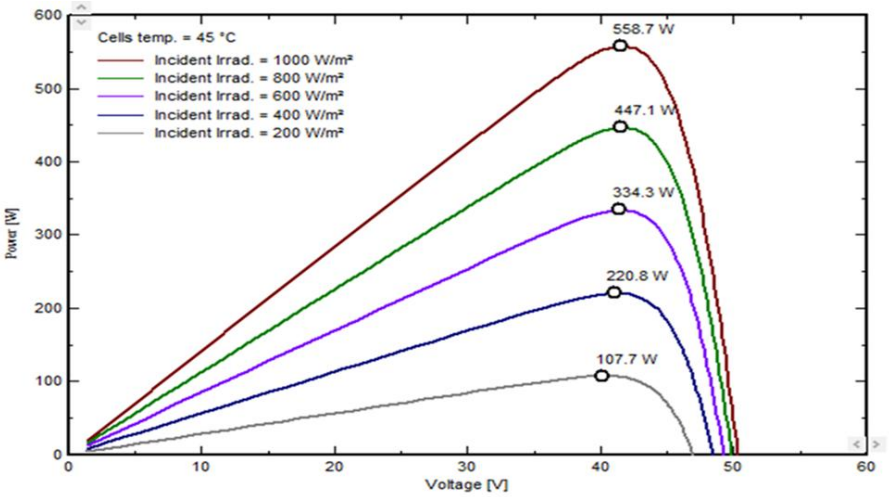

Fig. 20. The P-V curves of the JA (JAM78S30-600MR) photovoltaic module at various levels of irradiance.

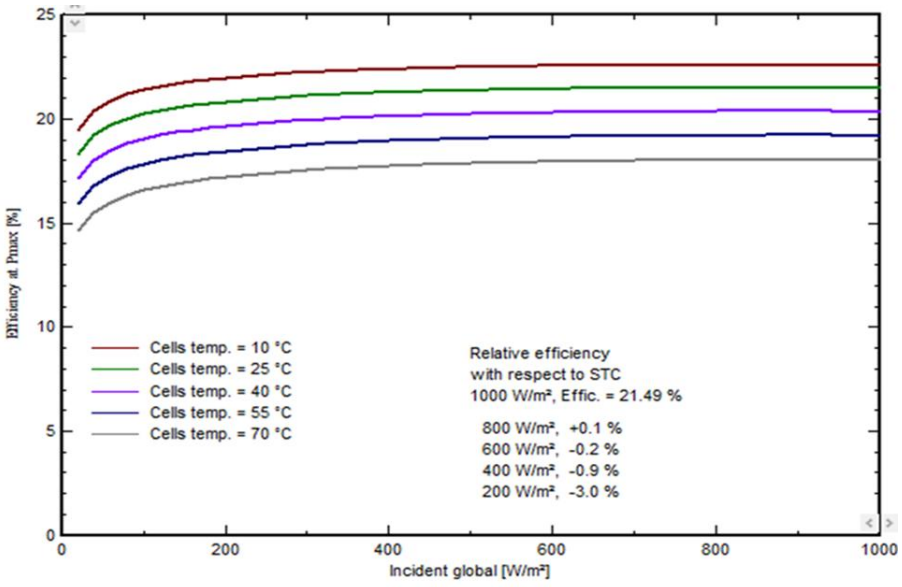

Fig. 21. JA PV module performance graphs at various irradiance and temperature conditions.

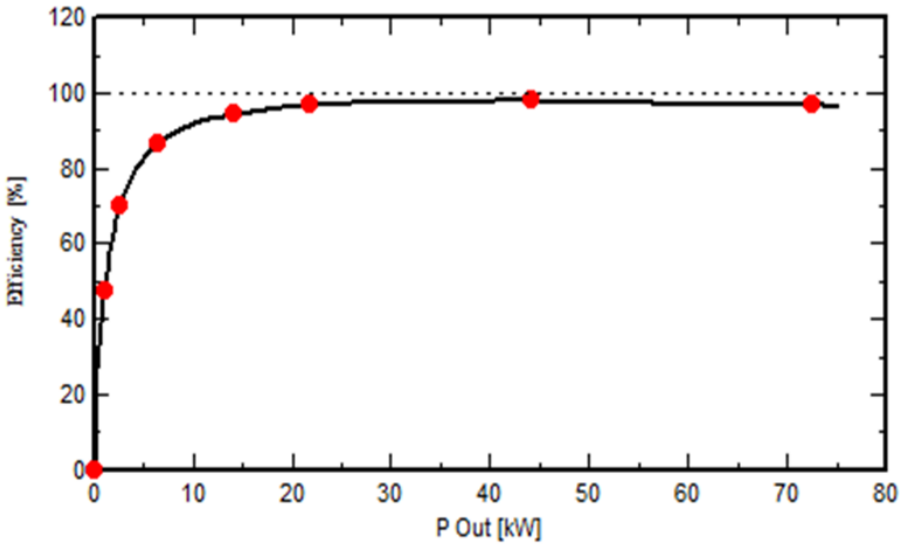

Fig. 22. Veichi IS23, 75-kW Inverter efficiency.

3.12. Flow rate and quantity of water being pumped

The average flow rate of the pump is 116 m^3/h, as illustrated in Fig. 23. The monthly average volume of water pumped was 30,880.8 m^3, leading to an overall yearly volume of water pumped totaling 370,571 m^3. Considering the total monthly requirement of 30,872.9 m^3, it is evident that the system adequately meets the water demand with a slight surplus in water production. This provides a favorable buffer in the event of future increases in water requirements or a reduction in well flow.

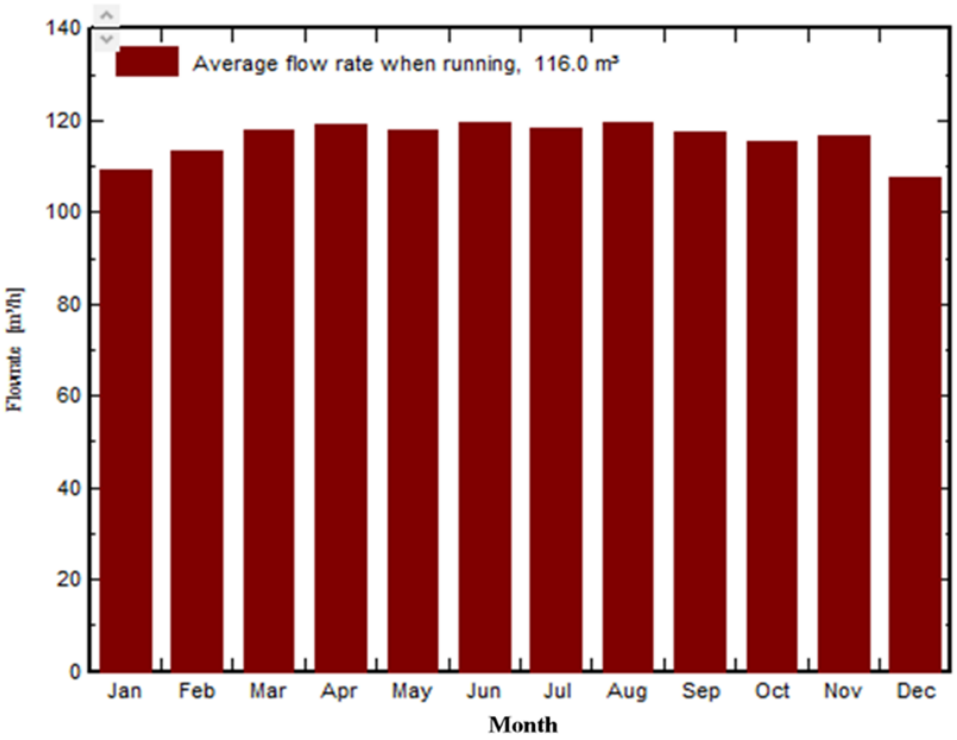

Fig. 23. Submersible Pump flow rate.

3.13. System balance and losses (loss diagram)

The loss diagram for the PV water pumping system is presented in Fig. 24. The sequential illustration of losses in the solar energy system can be seen in the loss diagram. Solar PV systems undergo several types of losses, which encompass module mismatch loss, ohmic wiring loss, module quality loss, threshold power loss in the converter, operational converter loss, charge/discharge current efficiency loss, battery efficiency loss,

and threshold power loss in the inverter (Rout and Kulkarni, 2020; Agyekum et al., 2022). The most significant system losses were array losses from heat (9.83%), mismatch losses (2.15%), unused energy (tank full) (7.80%), operational converter losses (3.21%), drawdown head losses (17.91%), and friction head losses (3.38%). Following the assessment of the losses, the quantity of water pumped was calculated. The volume of water pumped amounted to 370,570 m^3, while the necessary volume was 370,475 m^3.

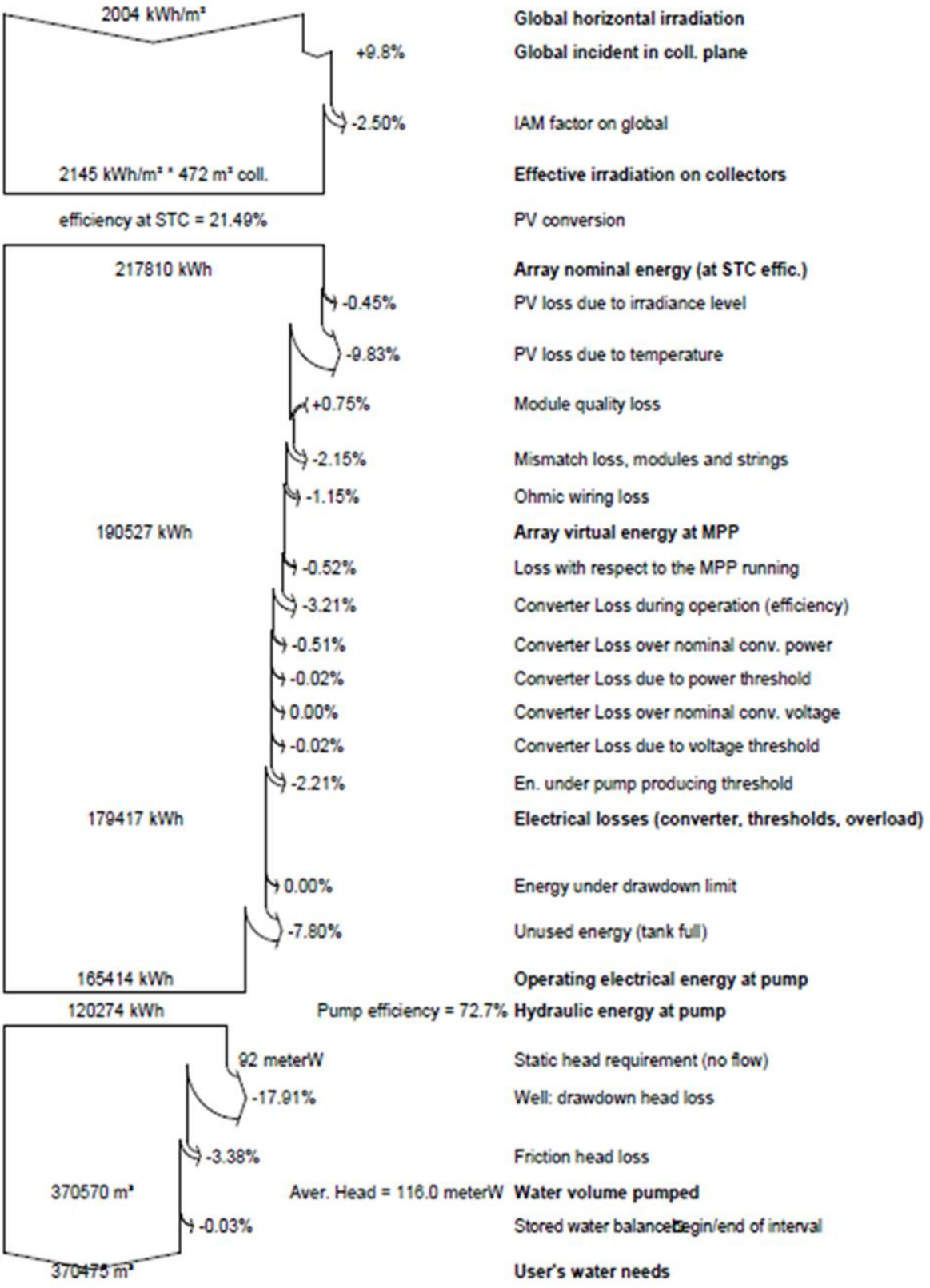

Fig. 24. loss diagram.

4. Conclusions

This study was conducted to design and simulate a 101.4 kW photovoltaic water pumping system using PVsyst 7.4 software to supply clean water to a farm experiencing power and water shortages. The findings of this study culminate in the following conclusions:

- The errors in the design and component selection were corrected using PV SYST software, leading to the creation of an optimal design for the solar water pumping system.
- Based on the results of the simulation, it was possible to verify the efficiency, reliability, and ability of the system to meet water requirements.
- The effective solar radiation on the collector plane was 2145 kWh/m², whereas the nominal power output of the array was 461.46 kWh/m², indicating an efficiency value of 21.5% for the array.
- Inverter efficiency reached 96%, signifying that it encountered appropriate inputs and outputs from panels and loads.
- The electrical energy consumed by the pumping unit was 165,414 kWh, whereas its hydraulic energy was 120,274 kWh, yielding a pump efficiency of 72.7%.
- The volume of pumped water was 370,570 m^3, and the required volume was 370,475 m^3. It is evident that the system adequately meets the water demand with a slight surplus in water production. This provides a favorable buffer in the event of future increases in water requirements or reductions in well flow.
- Furthermore, the performance ratio for the majority of the year was approximately 74%, which is satisfactory.

References

Abbood Al-Khazzar, A.A., 2018. A Theoretical Detailed Analysis for a Proposed 5kW PV Grid-Connected System Installed in Iraq Using PVsyst Tool. Iranica Journal of Energy & Environment, 9(2), 105-113. https://doi.org/10.5829/ijee.2018.09.02.05.

Aghaei, M., Eskandari, A., Vaezi, S., Chopra, S.S., 2020b. Solar PV power plants. In Photovoltaic solar energy conversion (pp. 313-348). Academic Press. https://doi.org/10.1016/B978-0-12-819610-6.00010-7.

Aghaei, M., Kumar, N.M., Eskandari, A., Ahmed, H., de Oliveira, A. K.V., Chopra, S.S., 2020a. Solar PV systems design and monitoring. In Photovoltaic solar energy conversion (pp. 117-145). Academic Press. https://doi.org/10.1016/B978-0-12-819610-6.00005-3.

Agyekum, E.B., Mehmood, U., Kamel, S., Shouran, M., Elgamli, E., Adebayo, T.S., 2022. Technical performance prediction and employment potential of solar PV systems in cold countries. Sustainability, 14(6), 3546. https://doi.org/10.3390/su14063546.

Ahmed, N.M., Hassan, A.M., Kassem, M.A., Hegazi, A.M., Elsaadawi, Y.F., 2023. Reliability and performance evaluation of a solar PV-powered underground water pumping system. Scientific Reports, 13(1), 14174. https://doi.org/10.1038/s41598-023-41272-5.

Ahmed, R., Sreeram, V., Mishra, Y., Arif, M.D., 2020. A review and evaluation of the state-of-the-art in PV solar power forecasting: Techniques and optimization. Renewable and sustainable energy reviews, 124, 109792. https://doi.org/10.1016/j.rser.2020.109792.

Ali, M.F., Sarker, N.K., Hossain, M.A., Alam, M.S., Sanvi, A.H., Syam Sifat, S.I., 2023. Techno-economic feasibility study of a 1.5 MW grid-connected solar power plant in Bangladesh. Designs, 7(6), 140. https://doi.org/10.3390/designs7060140.

Aliyu, M., Hassan, G., Said, S.A., Siddiqui, M.U., Alawami, A.T., Elamin, I.M., 2018. A review of solar-powered water pumping systems. Renewable and Sustainable Energy Reviews, 87, 61-76. https://doi.org/10.1016/j.rser.2018.02.010.

Ameur, A., Berrada, A., Loudiyi, K., Adomatis, R., 2021. Performance and energetic modeling of hybrid PV systems coupled with battery energy storage. In Hybrid Energy System Models (pp. 195-238). Academic Press. https://doi.org/10.1016/B978-0-12-821403-9.00008-1.

Ardizzon, G., Cavazzini, G., Pavesi, G., 2014. A new generation of small hydro and pumped-hydro power plants: Advances and future challenges. Renewable and Sustainable Energy Reviews, 31, 746-761. https://doi.org/10.1016/j.rser.2013.12.043.

Chandel, M., Agrawal, G.D., Mathur, S., Mathur, A., 2014. Techno-economic analysis of solar photovoltaic power plant for garment zone of Jaipur city. Case Studies in Thermal Engineering, 2, 1-7. https://doi.org/10.1016/j.csite.2013.10.002.

Cosgun, A.E., Demir, H., 2024. Investigating the Effect of Albedo in Simulation-Based Floating Photovoltaic System: 1 MW Bifacial Floating Photovoltaic System Design. Energies, 17(4), 959. https://doi.org/10.3390/en17040959.

Dirnberger, D., 2017. Photovoltaic module measurement and characterization in the laboratory. In The Performance of Photovoltaic (PV) Systems (pp. 23-70). Woodhead Publishing. https://doi.org/10.1016/B978-1-78242-336-2.00002-1.

El Abagy, A., Emeara, M., AbdelGawad, A., 2021. Orientation-optimization simulation for solar photovoltaic plant of Cairo international airport. The Egyptian International Journal of Engineering Sciences and Technology, 33(Mechanical Engineering), 45-68. https://dx.doi.org/10.21608/eijest.2021.56964.1035.

Elbelkemy, M.S., Zabady, F.E., Darwish, W., 2025. Utilizing geographic information systems (GIS) in designing irrigation networks. Al-Azhar Journal of Agricultural Engineering, 8(1). https://doi.org/10.21608/azeng.2024.323320.1019.

Elsaadawi, Y.F., Gwaily, S.A.E.M., Darwish, E.A., 2025. Design and simulation of a standalone solar energy system by PV SYST. Unconventional Resources, 100195. https://doi.org/10.1016/j.uncres.2025.100195.

Elsaadawi, Y.F., Tayel, S.A., El-Maaty, A.E., Mostafa, E.M., 2023. Hydrophobic nanocoating impacts on the PV panels' current-voltage and power-voltage curves. Al-Azhar Journal of Agricultural Engineering, 4(1), 1-9. https://doi.org/10.21608/azeng.2022.278933.

Elwakeel, A.E., Ahmed, S.F., Zein Eldin, A.M., Nasrat, L., 2021. Design of a novel electronic circuit for AC induction motor speed control. Al-Azhar Journal of Agricultural Engineering, 1(1), 49-55. https://dx.doi.org/10.21608/azeng.2021.209949.

Espina, R.U., Enano, N.H., Descalsota, E.E., Occidental, J.T., 2022. Modeling and simulation of a 48-kW off-grid solar-PV power system using PVSyst.

Faiz, F.U.H., Shakoor, R., Raheem, A., Umer, F., Rasheed, N., Farhan, M., 2021. Modeling and analysis of 3 MW solar photovoltaic plant using PVSyst at Islamia University of Bahawalpur, Pakistan. International journal of Photoenergy, 2021(1), 6673448. https://doi.org/10.1155/2021/6673448.

Gao, Z., Li, S., Zhou, X., Ma, Y., 2016, August. An overview of PV system. In 2016 IEEE International Conference on Mechatronics and Automation (pp. 587-592). IEEE. https://doi.org/10.1109/ICMA.2016.7558629.

García, R.G., Gamboa, G.O., Antuñano, M.A.Z., Ramírez, M.C., García, S.G., López, L.V., Pérez, E.L.O., 2021. Sizing photovoltaic systems interconnected to the grid in the industry. Maejo International Journal of Energy and Environmental Communication, 3(2), 32-37. https://doi.org/10.54279/mijeec.v3i2.245840.

Khamisani, A.A., 2019. Design methodology of off-grid PV solar powered system (A case study of solar powered bus shelter). Goolincoln Avenue Charleston, IL: Eastern Illinois University. https://kh.aquaenergyexpo.com/wp-content/uploads/2023/08/Design-Methodology-of-Off-Grid-PV-Solar-Powered-System.pdf.

Kumar, N.M., Kumar, M.R., Rejoice, P.R., Mathew, M., 2017. Performance analysis of 100 kWp grid connected Si-poly photovoltaic system using PVsyst simulation tool. Energy Procedia, 117, 180-189. https://doi.org/10.1016/j.egypro.2017.05.121.

Kumar, R., Rajoria, C.S., Sharma, A., Suhag, S., 2021. Design and simulation of standalone solar PV system using PVsyst Software: A case study. Materials Today: Proceedings, 46, 5322-5328. https://doi.org/10.1016/j.matpr.2020.08.785.

Muhsen, D.H., Khatib, T., Nagi, F., 2017. A review of photovoltaic water pumping system designing methods, control strategies and field performance. Renewable and Sustainable Energy Reviews, 68, 70-86. https://doi.org/10.1016/j.rser.2016.09.129.

Muzaffar, C.B., Iqbal, M.T., 2020, November). Design and analysis of off grid solar system for DC load of a house in Pakistan. In 2020 11th IEEE Annual Information Technology, Electronics and Mobile Communication Conference (IEMCON) (pp. 0804-0807). IEEE. https://doi.org/10.1109/IEMCON51383.2020.9284863.

Nag, S.K., Gangopadhyay, T.K., 2022. Design of LED lighting system using solar powered PV cells for a proposed business complex. Scientific Reports, 12(1), 13289. https://doi.org/10.1038/s41598-022-17353-2.

Ramoliya, J.V., 2015. Performance evaluation of grid-connected solar photovoltaic plant using PVSYST software. Journal of Emerging Technologies and Innovative Research (JETIR), 2(2), 7. https://www.jetir.org/view?paper=JETIR1502036.

Rout, K.C., Kulkarni, P.S., 2020, February. Design and performance evaluation of proposed 2 kW solar PV rooftop on grid system in Odisha using PVsyst. In 2020 IEEE International Students' Conference on Electrical, Electronics and Computer Science (SCEECS) (pp. 1-6). IEEE. https://doi.org/10.1109/SCEECS48394.2020.124.

Samuel, R., Kumar, P.V., Jayaraj, J., 2021. Assessment Of Solar Energy Capacity And Performance Evaluation Of A Standalone Pv System With Pvsyst. Turkish Journal of Computer and Mathematics Education, 12(13), 2384-2390. https://www.proquest.com/scholarly-journals/assessment-solar-energy-capacity-performance/docview/2623932837/se-2.

Serat, Z., Fatemi, S.A.Z., Shirzad, S., 2023. Design and economic analysis of on-grid solar rooftop PV system using PVsyst software. Archives of Advanced Engineering Science, 1(1), 63-76. https://doi.org/10.47852/bonviewAAES32021177.

Tayel, S.A., Abu El-Maaty, A.E., Mostafa, E.M., Elsaadawi, Y.F., 2022. Enhance the performance of photovoltaic solar panels by a self-cleaning and hydrophobic nanocoating. Scientific reports, 12(1), 21236. https://doi.org/10.1038/s41598-022-25667-4.

Tayel, S.A., Lithy, A.M., Hegazi, A., El-Saadawi, Y.F., 2019. Performance evaluation of water pumping system powered by solar energy. Misr Journal of Agricultural Engineering, 36(1), 283-302. https://dx.doi.org/10.21608/mjae.2019.94460.

Usman, Z., Tah, J., Abanda, H., Nche, C., 2020. A critical appraisal of pv-systems' performance. Buildings, 10(11), 192. https://doi.org/10.3390/buildings10110192.

Verma, S., Mishra, S., Chowdhury, S., Gaur, A., Mohapatra, S., Soni, A., Verma, P., 2021. Solar PV powered water pumping system–A review. Materials Today: Proceedings, 46, 5601-5606. https://doi.org/10.1016/j.matpr.2020.09.434.

Yadav, A.K., Yadav, V., Malik, H., Khargotra, R., Singh, T., 2024. Design of novel IoT-based solar powered PV pumping systems for agricultural applications in diverse climatic zones of India. Results in Engineering, 23, 102584. https://doi.org/10.1016/j.rineng.2024.102584.

تطوير ومحاكاة نظام طاقة شمسية باستخدام برمجية PV SYST

يوسف فايز السعداوي [١]، محمد محمد ممدوح جعيصه [١]، إيناس لقمان عبد اللطيف سالم [٢]، علوان علي درويش [١]

[١] قسم هندسة تصنيع المنتجات الزراعية، كلية الهندسة الزراعية، جامعة الأزهر، القاهرة، مصر.

[٢] معهد بحوث الهندسة الزراعية، مركز البحوث الزراعية، مصر.

الملخص العربي

وفرة الطاقة الشمسية غالباً تصاحبها ندرة مصادر الطاقة الأخرى والمياه النظيفة، كما هو الحال في المناطق الصحراوية. وتُعدّ الأوراق البحثية المنشورة في مجلات محكمة تتناول تصميم ومحاكاة أنظمة الطاقة الشمسية باستخدام الحزمة البرمجية PV SYST نادرة. لذلك، تم إجراء هذه الدراسة لتصميم ومحاكاة نظام ضخ مياه جوفية يعمل بالطاقة الشمسية بقدرة ١٠١,٤ كيلوواط باستخدام برمجية PV SYST، بهدف تزويد مزرعة تعاني من نقص في موارد المياه والطاقة، بالمياه اللازمة للمرافق والعمليات الزراعية. بالإضافة إلى ذلك، ومن خلال محاكاة النظام لمدة عام كامل باستخدام برنامج PV SYST، تم جمع معلومات حول خسائر النظام، ومكوناته غير المناسبة، وأخطاء التصميم. ومن خلال معالجة هذه المشكلات قبل التركيب، يُمكن توفير الوقت والجهد والموارد. بلغ قيمة الإشعاع الشمسي الفعال على سطح مصفوفة الألواح الشمسية ٢١٤٥ كيلوواط ساعة/م٢، بينما سجلت الطاقة الإسمية ٤٦١,٤٦ كيلوواط ساعة/م٢. وهذا يوضح كفاءة المصفوفة، والتي بلغت ٢١,٥٪ في ظل ظروف الاختبار (STC). وعندما وصلت الطاقة الإسمية للمصفوفة ٢١٧٨١٠ كيلوواط ساعة، كانت قيمة الطاقة الهيدروليكية ١٢٠٢٧٤ كيلوواط ساعة. ويعود هذا الاختلاف إلى الخسائر، وأهمها خسائر المصفوفة بسبب ارتفاع درجات الحرارة بمعدل ٩,٨٣٪ وخسائر العاكس أثناء التشغيل بمعدل ٣,٢١٪. سجلت الطاقة الكهربائية التشغيلية للمضخة ١٦٥٤١٤ كيلوواط ساعة، وبلغت طاقتها الهيدروليكية ١٢٠٢٧٤ كيلوواط ساعة، ما نتج عنه كفاءة مضخة بنسبة ٧٢,٧٪. وبلغ حجم المياه التي تم ضخها ٣٧٠٥٧٠ متر مكعب/سنة، في الوقت الذي كانت فيه متطلبات المياه ٣٧٠٤٧٥ متر مكعب/سنة، مما يشير إلى أن النظام كان قادرًا على تلبية متطلبات المياه. بلغت نسبة الأداء ٧٤,١٪، وهي نسبة مُرضية. وهذا يدل على صحة وكفاءة تصميم نظام الطاقة الكهروضوئية وموثوقيته.